Available online at www.sciencedirect.com

ScienceDirect

Engineering Fracture Mechanics 74 (2007) 1904–1916

Engineering Fracture Mechanics

www.elsevier.com/locate/engfracmech

Determination of interfacial fracture toughness of bone–cement interface using sandwich Brazilian disks

J. Tong *, K.Y. Wong, C. Lupton

Department of Mechanical and Design Engineering, University of Portsmouth, Anglesea Road, Anglesea Building, Portsmouth PO1 3DJ, UK

Received 8 December 2005; received in revised form 21 February 2006; accepted 24 February 2006
Available online 18 April 2006

Abstract

The long-term stability of cemented total hip replacements critically depends on the lasting integrity of the bond between bone and bone cement. Conventionally, the bonding strength of bone–cement is obtained by mechanical tests that tend to produce a large variability between specimens and test methods. In this work, interfacial fracture toughness of synthetic bone–cement interface has been studied using sandwiched Brazilian disk specimens. Experiments were carried out using polyurethane foams as substrates and a common bone cement as an interlayer. Selected loading angles from 0° to 25° were used to achieve full loading conditions from mode I to mode II. Finite element analyses were carried out to obtain the solutions for strain energy release rates at given phase angles associated with the experimental models. The effects of crack length on the measured interfacial fracture toughness were examined. Microscopic studies were also carried out to obtain the morphology of the fractured interfaces at selected loading angles.

The implication of the results on the assessment of fixation in acetabular replacements is discussed in the light of preliminary work on bovine cancellous bone–cement interface.

1. Introduction

The lasting integrity of the bond between bone and bone cement is of critical importance to the success of cemented joint replacements. Late failure in the absence of infection, known as ''aseptic loosening'', is often associated with mechanical failures of the cement–bone interface [1,2] in cemented arthroplasty. Multiple biological and mechanical factors may be responsible for aseptic loosening, although the initiation of failures during the early period post operation may well be mechanical [3–5].

The bonding strength of interfaces in cemented arthroplasty systems has been evaluated using conventional mechanical testing, such as reported in [5–10]. The most comprehensive study of bone–cement interface to day was carried out by Mann and his associates [5,8–10], including modelling the tensile behaviour of the cement–bone interface [8], mechanical strength of the bone–cement interface in shear and tension [9], mixed mode [5]

* Corresponding author.
E-mail address: jie.tong@port.ac.uk (J. Tong).

0013-7944
doi:10.1016/j.engfracmech.2006.02.014

and creep-fatigue damage [10]. Although of considerable value for orthopaedic research, the measured strength of the interface is found to be very sensitive to material combination, specimen geometry and fixture conditions [5,11]. There is a large variation in the results between specimens due to the difference in the amount of cement infiltration into bone and variations in human cadaveric bone tissues [5]. A variety of failure mechanisms has also been observed [11] during the separation process of bone–cement interface, such that the failure characteristics cannot be uniquely quantified by a bonding property.

A fracture mechanics approach may be adopted to determine the interfacial fracture toughness in the presence of defects at the interface. This method seems to be more appropriate since micro-defects may form during the process of cement application and curing, and as a result of subsequent cyclic loadings in routine activities. Both material mismatch and mixture of loading modes may be characterised by a phase angle, ψ, and interfacial fracture toughness, G_{IC}, of a given bimaterial system is known to vary significantly with ψ. A number of specimen geometries have been developed as suitable candidates for interfacial fracture toughness testing [12–15]. Sandwiched compact tension specimens [12] were used to produce predominantly mode I loading conditions with a phase angle $\psi \approx 0°$; while four-point bend arrangements provided results within the mid-range $\psi \approx 35°$–$60°$ [13]. Interfacial fracture toughness between cortical bone and cement [12] was also studied by Swain et al. [14] using a four-point bend test arrangement, although the same quantity has not been reported between cancellous bone and cement. This latter information is critical, as in joint replacement operations, subchondral bones are normally removed to facilitate mechanical interlocking between cancellous bones and cement. Understanding the failure mechanisms and quantify the interfacial fracture toughness between cancellous bone and cement are therefore imperative, if the problem of aseptic loosening in cemented arthroplasty is to be solved.

Ideally, a test specimen should cover a range of phase angles so that a variety of material mismatch and mixed mode loading conditions may be characterised. Brazilian disk specimen [15] is such a convenient arrangement that allows the measurement of interfacial fracture toughness as a function of loading angle θ to achieve loading conditions from mode I to mode II. A homogeneous specimen is in mode I when loaded in $\theta = 0°$, and mode II when loaded in $\theta \approx 25°$. Finite element solutions for stress intensity factors are available for disks with dissimilar halves [16]. Alternatively, a sandwich specimen may be obtained by using an interlayer to glue two identical halves of substrates, as shown in Fig. 1. The sandwiched specimens have the advantage that the residual stresses in the layer do not affect the stress intensities [17], hence can be ignored

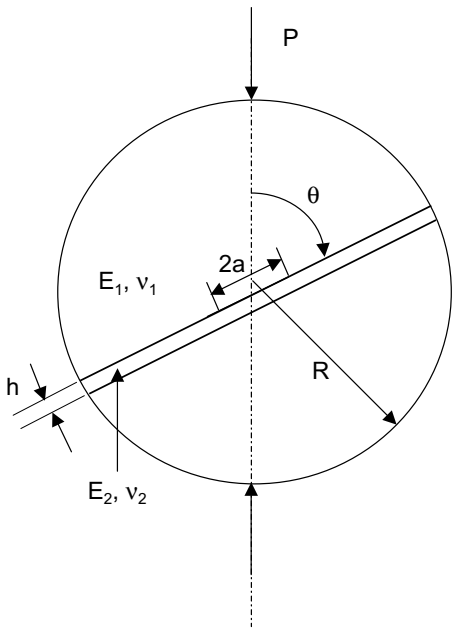

Fig. 1. The geometry and loading of a sandwich Brazilian disk.

when evaluating interfacial fracture toughness. The specimen has been successfully used in the determination of interfacial toughness between substrates including aluminium, brass, steel and plexiglass and interlayer epoxy, although the stress intensity factor solutions for a homogeneous disk were used in [17], under the assumption that the interlayer was much smaller than the other characteristic dimensions.

Sandwiched Brazilian disk specimens were chosen for the present study to reflect the nature of loading at the bone–cement interface within the acetabular prosthetic system, which is a mixture of compression and shear [18], as opposed to primarily bending in femoral components [14]. The aims of this work were to explore the feasibility of Brazilian disk specimens in the determination of interfacial fracture toughness of cancellous bone–cement interface, and to develop a methodology that may be used in the assessment of the integrity of acetabular fixation based on fracture mechanics concepts. Due to the appreciable thickness of the cement interlayer representative of cement mantles used in acetabular replacements, finite element solutions for stress intensity factors and strain energy release rate of a sandwich disk were obtained for selected crack lengths and moduli ratios. Experiments were carried out using solid polyurethane foams, as cancellous bone analogous materials and bone cement. The effects of crack length on the measured interfacial fracture toughness were examined. Fracture mechanisms of the interfaces were studied using microscopic methods. The results were discussed in the light of preliminary experimental results on bovine cancellous bone–cement interface.

2. Basic interfacial fracture mechanics

For a plane strain interfacial crack problem, the stress field for a semi-infinite interface crack separating two dissimilar isotropic elastic materials has the form [19]

$$\sigma_{22} + \mathrm{i}\sigma_{12} = (K_{\mathrm{I}} + \mathrm{i}K_{\mathrm{II}})(2\pi r)^{1/2} r^{\mathrm{i}\varepsilon}, \tag{1}$$

where r is the radial distance from the crack tip, $\mathrm{i} = \sqrt{-1}$ and ε is the oscillation index,

$$\varepsilon = \frac{1}{2\pi} \ln\left(\frac{1-\beta}{1+\beta}\right), \tag{2}$$

and β is a Dundurs' parameter

$$\beta = \frac{1}{2} \frac{G_1(1-2\nu_2) - G_2(1-2\nu_1)}{G_1(1-\nu_2) + G_2(1-\nu_1)}, \tag{3}$$

where G_1,G_2 are shear moduli, $G_1 = \frac{E_1}{2(1+\nu_1)}$, $G_2 = \frac{E_2}{2(1+\nu_2)}$; E_1,ν_1 are the elastic constants for material 1, while E_2,ν_2 are the elastic constants for material 2.

When $\beta \neq 0$, thus $\varepsilon \neq 0$, K_{I} and K_{II} do not strictly measure the normal and shear components of the stress intensity, as the two components do not decouple independent of r due to the term $r^{\mathrm{i}\varepsilon} = \exp(\mathrm{i}\varepsilon \ln r)$. As a remedy, the ratio of the shear and the normal components may be considered at a fixed reference distance L_0 and Eq. (1) becomes

$$\sigma_{22} + \mathrm{i}\sigma_{12} = \frac{1}{\sqrt{2\pi r}} (K_{\mathrm{I}} + \mathrm{i}K_{\mathrm{II}}) L_0^{\mathrm{i}\varepsilon} \left(\frac{r}{L_0}\right)^{\mathrm{i}\varepsilon}, \tag{4}$$

and the phase angle at the reference distance L_0 is

$$\psi = \tan^{-1} \frac{\mathrm{Im}[KL_0^{\mathrm{i}\varepsilon}]}{\mathrm{Re}[KL_0^{\mathrm{i}\varepsilon}]} = \tan^{-1} \left[\left(\frac{\sigma_{12}}{\sigma_{22}}\right)_{L=L_0}\right]. \tag{5}$$

The relation between the energy release rate and the magnitude of stress intensity factors $|K|$ may be obtained [20]:

$$G = \frac{1}{2}(1-\beta^2)\left[\frac{1-\nu_1^2}{E_1} + \frac{1-\nu_2^2}{E_2}\right]|K|^2, \tag{6}$$

$$|K| = \sqrt{K_1^2 + K_2^2}. \tag{7}$$

For most of the dissimilar material systems, the choice of the fixed distance is not critical [19]. If necessary, the loading phase angle at a distance of $L_1 \neq L_0$ may be readily obtained by a simple transformation

$$\psi_{L_1} = \psi_{L_0} + \varepsilon \ln \frac{L_1}{L_0}. \tag{8}$$

3. Finite element analysis

3.1. Brazilian disk specimen

3.1.1. Homogeneous disk

A homogeneous circular disk of radius R, with a centre crack of length $2a$, was presented by Atkinson et al. [15], where explicit formulae for stress intensity factors K_{I} and K_{II} were given as

$$\begin{aligned} K_{\mathrm{I}} &= \frac{P}{\pi BR}\sqrt{\pi a} f_{\mathrm{I}}, \\ K_{\mathrm{II}} &= \frac{P}{\pi BR}\sqrt{\pi a} f_{\mathrm{II}}, \end{aligned} \tag{9}$$

where P is the applied load, B and R are the thickness and the radius of the disk, respectively, and f_{I} and f_{II} are functions of the loading angle and relative crack size (a/R), and are available in polynomial forms [15].

3.1.2. Sandwich disk

Finite element analyses were carried out to evaluate the effect of a finite interlayer of dissimilar material on the solutions of stress intensity factors of a Brazilian disk. A finite element model was developed using ABAQUS 6.5 [21], with 13804 nodes and 3964 elements of 8-noded quadratic plane strain elements. The crack tips were specifically treated with collapsed 8-noded elements and an average size of 10 μm. The radius of the disk was taken as 20 mm, and selected rack lengths $2a = 2$, 5, 10, 15 and 20 mm were examined. Polyurethane foams, or sawbones, were used as substrates (material 1), while cement (material 2), of a 2 mm thickness, as an interlayer. The ratios of moduli of sawbone to cement, $E_1/E_2 = 0.2$, 0.5, 1, were examined, while $E_2 = 2$ GPa for cement. The Poisson's ratios for sawbone and cement were taken as 0.35 and 0.3, respectively. Contact elements were placed on the crack faces to prevent possible penetration of the crack flanks at large loading angles. The load was applied in x direction on a single node, while constraints in both x and y directions were placed on nodes at the opposite edge of the disk to avoid rigid body motion. The load and the constraints were maintained throughout the analyses while the disk was rotated to achieve loading angles of 0°, 5°, 10°, 15°, 20° and 25°. The finite element model of the sandwich disk is shown in Fig. 2.

3.2. Finite element results

The J-integral was computed along five integral contours. The first contour was the closest to the crack tip while the fifth the furthest. The values of the J-integral from the third to the fifth contour were identical to the fourth digit, hence the values of J-integral from the fifth contour were taken in all cases. The J-integrals were obtained for both left and right crack tips and the phase angles were evaluated as a function of the distance to the crack tip. The variation of the phase angle with the radial distance to the crack tip is shown in Fig. 3, for the case of $a/R = 0.25$. It seems evident that the variation of the phase angle with the distance to the crack tip is relatively small, consistent with the statement of Rice [19]. For consistency, the phase angles at 10 μm were taken for all cases in the following analyses. Fig. 4 shows the normalised strain energy release rates as a function of phase angle for selected ratios of moduli, where the values of the J-integral were normalised by a reference value, $J_0 = \frac{P^2}{2B^2R}\frac{1}{E_1'}$, where P, B, R are as defined in Eq. (9), E_1' is the plane strain tensile modulus for the sawbone,$E_1' = \frac{E_1}{1-\nu_1^2}$. The strength of strain energy release increases with the decrease of moduli ratio E_1/E_2. The

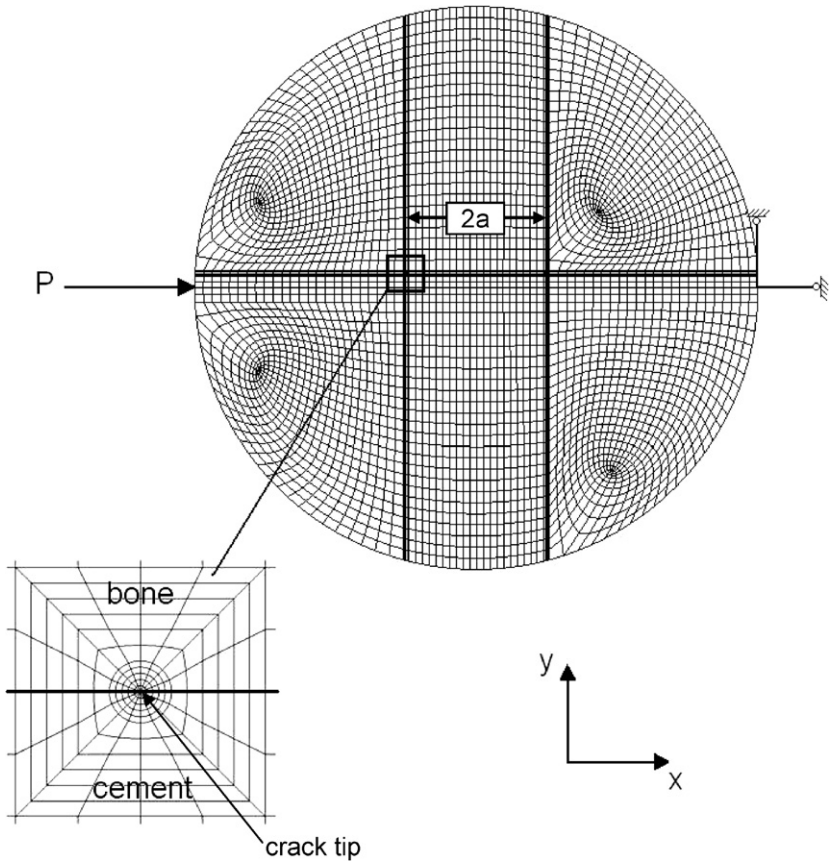

Fig. 2. Finite element model of the sandwich Brazilian disk with details of the interfacial crack tip elements.

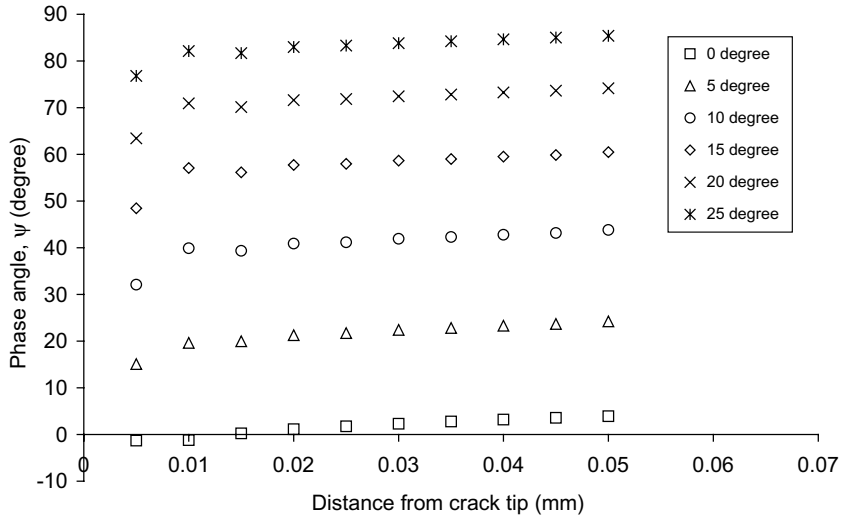

Fig. 3. Phase angle as a function of the radial distance to the crack tip for crack length-to-diameter ratio $a/R = 0.25$.

influence seems to be more pronounced at large phase angles, when shear deformation becomes dominant. At $\psi = 0°$, a difference of 24% was observed between the values of the J-integral for $E_1/E_2 = 0.2$ and 0.5; while at

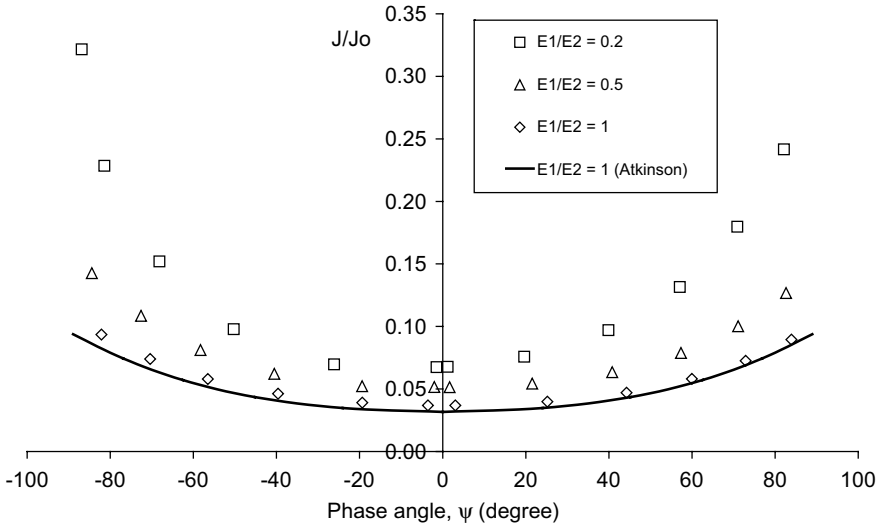

Fig. 4. Normalised strain energy release rates as a function of phase angle, the influence of moduli ratio E_1/E_2, where E_1 and E_2 are elastic moduli for bone and cement, respectively.

$\psi = 80°$, the difference increases to over 50% between the two cases. Results from a two-term polynomial fit of the solution of Atkinson et al. [15] are also included, and compared reasonably well with the present FE results for $E_1/E_2 = 1$.

The influence of crack length on the strain energy release rate was examined for $E_1/E_2 = 0.2$, and the results are shown in Fig. 5, where normalised strain energy release rates are presented as a function of phase angle for relative crack sizes, $a/R = 0.05$, 0.125, 0.25, 0.375 and 0.5 (Fig. 5a). Again, the increase in the normalised strain energy release rates with crack length becomes much more pronounced as the phase angle increases, consistent with the results from [16]. The relation between the phase angle and the loading angle for selected crack lengths is shown in Fig. 5b. The change of phase angle with the change of crack length seems to be relatively small. The relations shown in Fig. 5 were used in the calculation of the values of interfacial fracture toughness and the associated phase angles, once the fracture loads were obtained from the experiments.

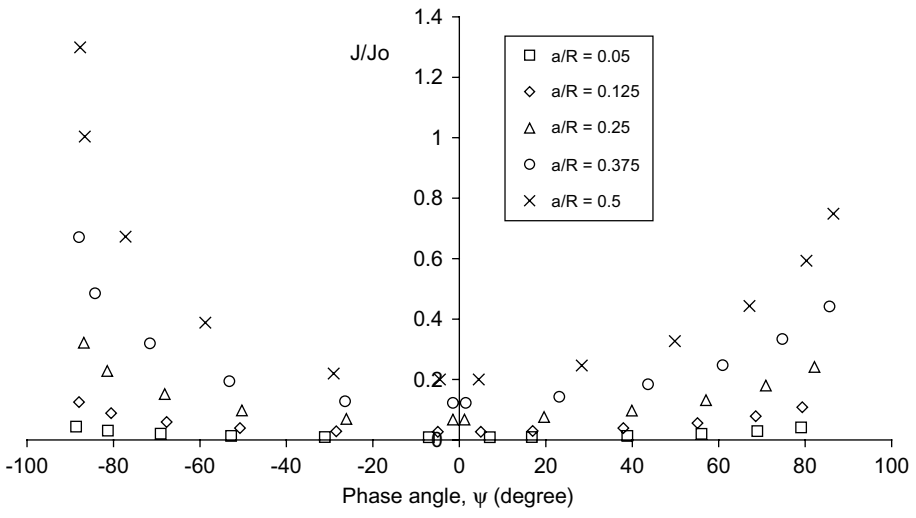

Fig. 5a. Normalised strain energy release rates as a function of phase angle for selected crack length-to-diameter ratios a/R.

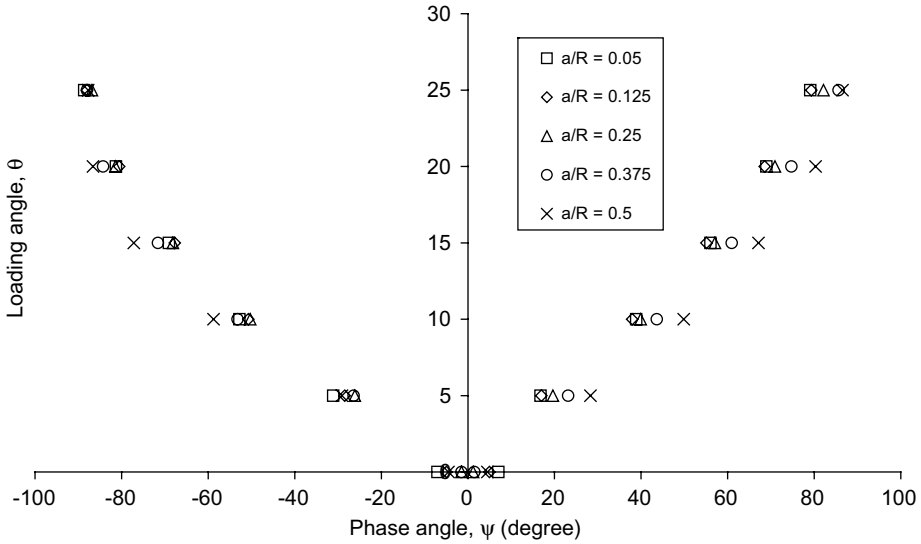

Fig. 5b. The relationship between the phase angles and the loading angles for selected crack length-to-diameter ratios a/R.

4. Experimental studies

4.1. Experimental methods

Solid rigid polyurethane foams (Pacific Research Laboratories) were used as an alternative medium for human cancellous bones. The solid foam blocks have a density of 0.64 g/cm^3 and are ''graded'' foams per ASTM standard F-1839 [22]. A commercial bone cement PMMA (CMW) was used for the study. The cement was mixed manually according to the recommended procedures, as in normal surgical operations. Rectangular foam blocks were marked for pre-determined initial crack lengths, $2a = 2$, 5, 10, 15, 20 mm, and the crack area was then protected using a piece of thin tape (0.05 mm) before the application of cement between this and another identical sized foam block. The use of thin tape is to ensure the sharpness of the crack tip, although work is to be carried out using fatigue pre-cracked samples so that the effect of crack tip morphology can be assessed. Pressure was applied and metal pins were used to ensure a uniform cement thickness of 2 mm until the cement set. The disks were then machined to the final size with a radius $R = 20 \pm 0.1$ mm and a thickness $B = 10 \pm 0.1$ mm.

The experiments were conducted at room temperature using a Hounsfield material testing machine (H20k-W). The load was applied under displacement control at a rate of 0.025 mm/s. Compressive force was applied at selected loading angles $\theta = 0°$, 5°, 10°, 15°, 20°, and 25°. All disks were measured for radius R and thickness B prior to testing and measured for crack length $2a$ post testing. Each experiment at a given crack length was repeated at least once. The deformation experienced in all disks appears to be mainly elastic until broken catastrophically and cracks propagated dynamically. Microscopic studies were carried out post fracture testing. Both intact and fractured interfaces at selected loading angles were mounted in resin, and the samples were prepared for microscopic examination.

4.2. Experimental results

Fig. 6 shows some of the typical load–displacement curves obtained at selected loading angles. The behaviour of the sandwich disks seems to be similar irrespective of the loading angles, with a characteristic non-linear region preceded a linear response towards fracture.

Fig. 7 shows the relation between the fracture load and the displacement at fracture for selected crack lengths. It seems that the fracture load increases with the decrease of the crack length, as well as the increase of the loading angle. The values of interfacial fracture toughness were obtained using the measured fracture

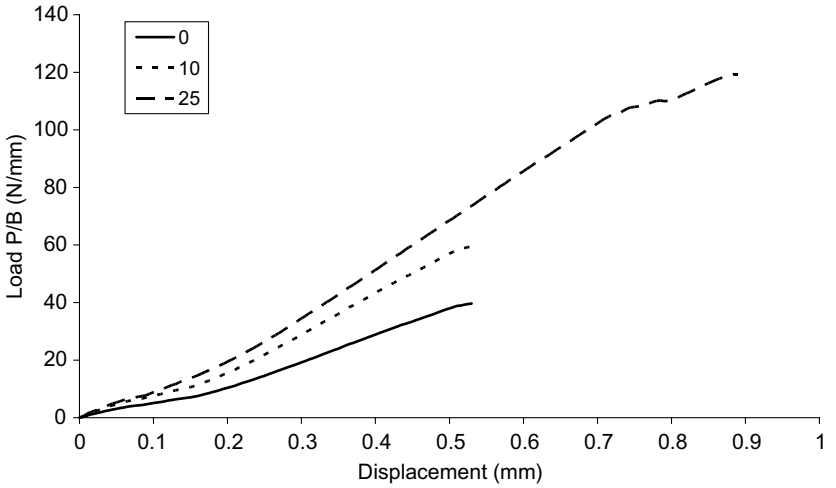

Fig. 6. Typical load-displacement curves obtained from tests of sandwich disks ($2a = 10$ mm) at selected loading angles $\theta = 0°$, 10° and 25°.

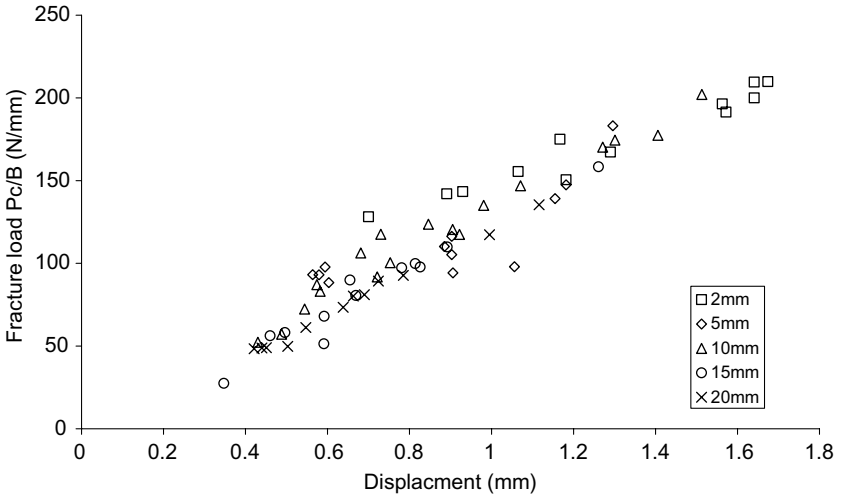

Fig. 7. Fracture loads as a function of the displacement at failure for selected crack lengths.

stresses, obtained by dividing the fracture load by the specimen thickness, and the calibration of the J-integral as a function of phase angle (Fig. 5). The results are presented in Fig. 8 for a range of crack lengths. Although the influence of crack length on the measured interfacial fracture toughness G_{IC} seems to be moderate at low phase angles, the effects of crack length on G_{IC} become more significant at high phase angles $\psi > 45°$, with artificially high values of fracture toughness obtained for long cracks ($2a > 10$ mm).

Microscopic examination showed that failures occurred almost exclusively at the desired bone–cement interface with little adhesion of cement or bone to the mating surface. Kinking out of the bone–cement interface with fracture in either the foam or the cement was very rare. Features of interest are shown in Fig. 9 for an intact interface and fractured interfaces. For the intact interface, satisfactory cement penetration into pores of the sawbone was clearly achieved (Fig. 9(a)); while for the fractured interfaces, the details of "pull-out" of cement pedicles from pores of the sawbone can be clearly observed. At loading angle $\theta = 0°$, little damage of the cement pedicles may be observed (Fig. 9(b)) due to the essentially mode I tensile loading experienced at the bone–cement interface. As the loading angle increases from 5°, 15° to 25°, shear deformation increases

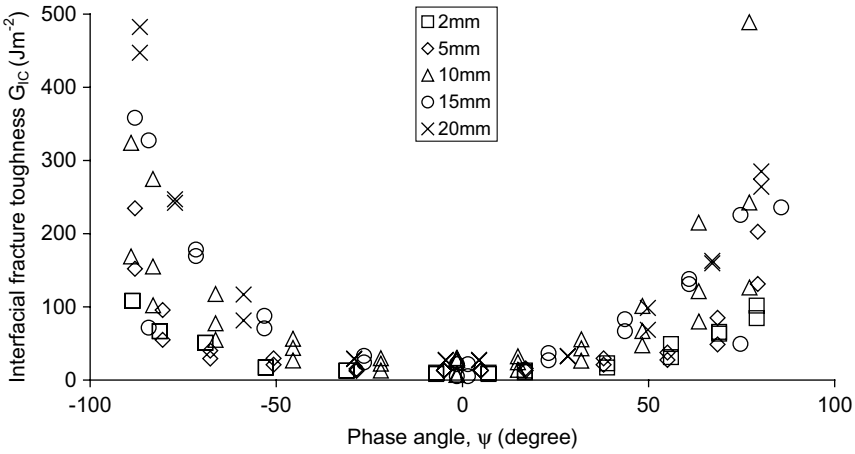

Fig. 8. Interfacial fracture toughness as a function of phase angle for selected crack lengths.

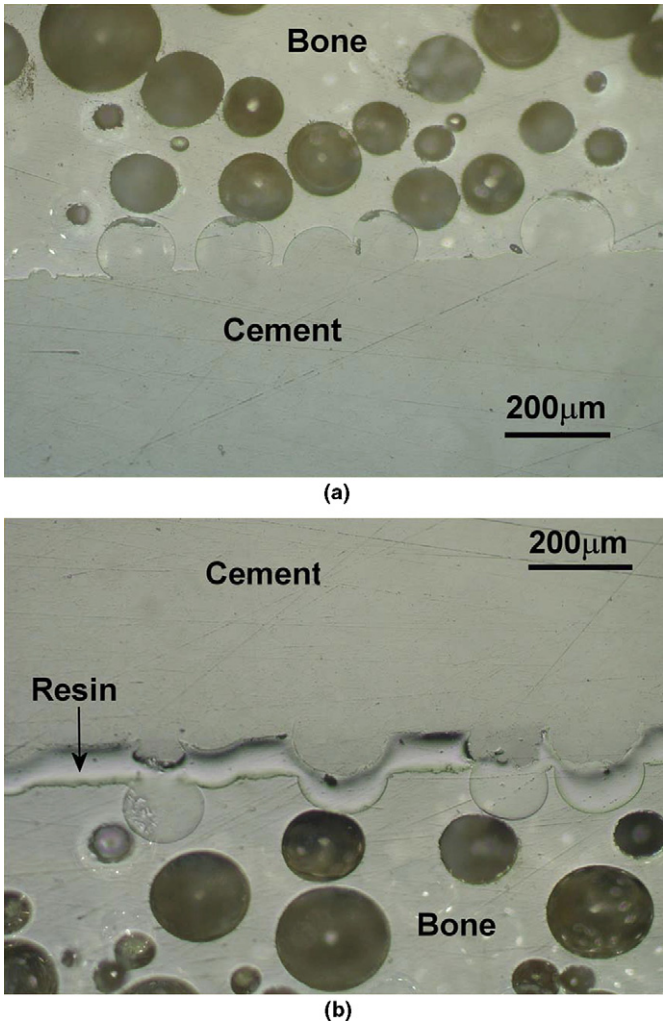

Fig. 9. Micrographs of the sawbone–cement interfaces ($a/R = 0.25$): (a) Intact interface; fractured interfaces at selected loading angles; (b) $\theta = 0°$; (c) $\theta = 5°$; (d) $\theta = 15°$ and (e) $\theta = 25°$.

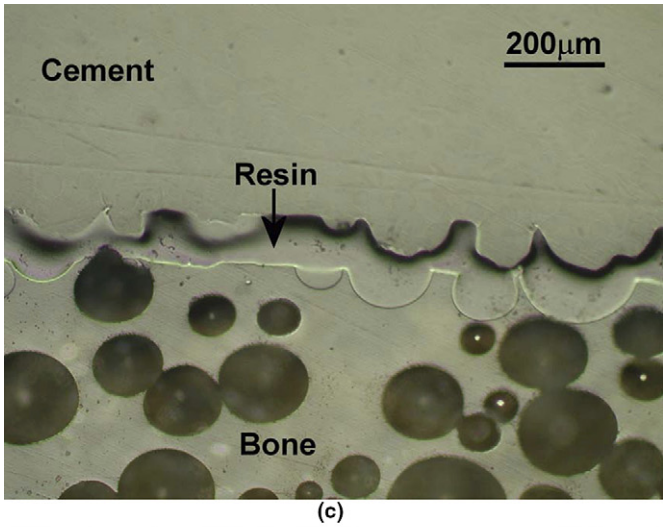

(c)

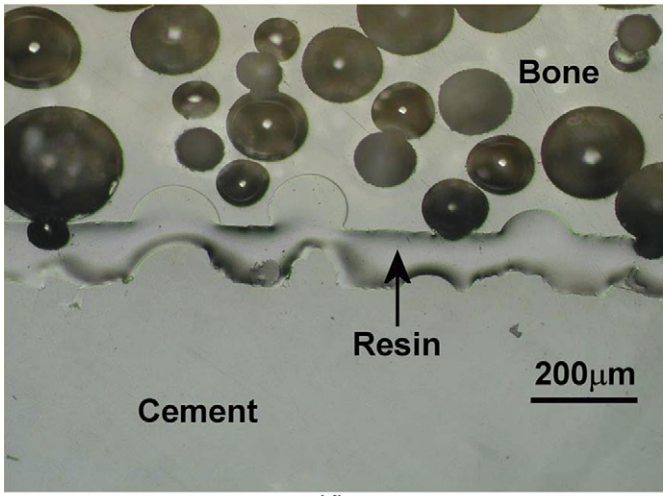

(d)

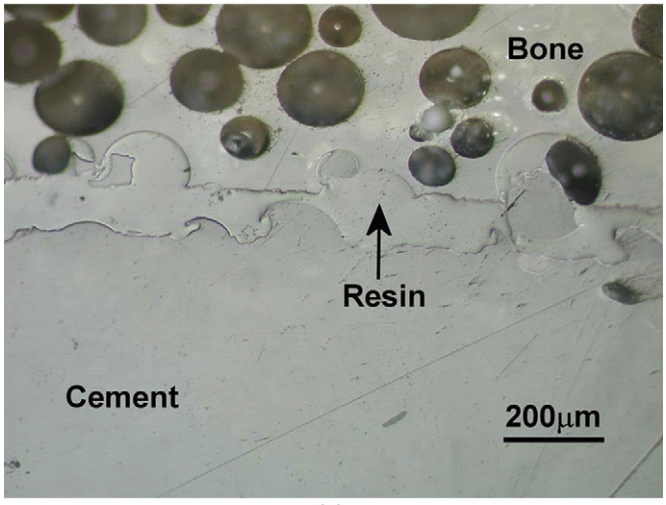

(e)

Fig. 9 (*continued*)

gradually. As a result, a progressively increased degree of shear damage was sustained by the cement pedicles during the mixed mode loading process, as shown in Fig. 9(c)–(e).

5. Discussion

The numerical analyses and the experimental results presented in this study demonstrate that interfacial fracture toughness of bone and cement may be evaluated using a sandwich Brazilian disk specimen. The magnitude of the overall strength of the interface is given by G_{IC}, while the phase angle ψ describes the ratio between the shear to tensile components acting at a fixed distance to the crack tip. Full range of phase angles from $-90°$ to $+90°$ may be achieved using such a specimen loaded at angles from 0° to 25°. This is clearly advantageous compared with other commonly used specimen geometries with more limited ranges of phase angles, such as $\psi \approx 0°$ for double-cantilever beam specimen [14]; $\psi < 18°$ for compact tension specimens [12] and $\psi \approx 45°$ for four-point bend specimens [14]. The only ambiguity may be that the crack growth from the two crack tips does not occur simultaneously for $\theta \neq 0°$. The left crack tip has a smaller, positive phase angle while the right tip has a negative but somewhat larger phase angle. It is likely that crack grows from the left tip first, although the actual difference seems to be inconsequential. There is a lack of material symmetry as the fracture toughness for a negative value of phase angle differs from that at the same positive value of the phase angle. This illustrates the importance of determining interfacial fracture toughness as a function of a full range of phase angles. The values of interfacial toughness should not be compared unless they are referred to the same phase angle. The consistency of fractures occurred at the desired bone–cement interfaces seems to suggest that valid interfacial fracture toughness results may be obtained using such a test arrangement.

The influence of moduli ratio on the strain energy release rate seems to be significant, particularly at large phase angles when shear deformation becomes predominant. This information is important in that the accuracy of the measured fracture toughness depends on the inputs of the moduli of the biomaterial system concerned. This is particularly so for large phase angles, when the difference between the values of the J-integral for $E_1 = 400$ MPa ($E_1/E_2 = 0.2$) and $E_1 = 1000$ MPa ($E_1/E_2 = 0.5$) can be as much as over 50% at $\psi \approx 80°$, as opposed to 24% at $\psi \approx 0°$ (Fig. 4). The modulus of the polyurethane foam is between 400 and 1000 MPa, corresponding to $E_1/E_2 = 0.2$ and 0.5, as examined in this study. These values are lower than the modulus of cortical bone (~17 GPa), but overlap the range of the modulus of cancellous bones [24]. Interface between cortical bone and cement is not of interest here, as the subchondral bone is almost always removed before the application of cement in acetabular replacements. Trabecular bones are known to be extremely heterogeneous and modulus can vary 100 fold within the same metaphysis [25] and are site and age dependent. Recent work from Keaveny et al. [24], however, reported that the elastic modulus from elderly human vertebral and young bovine tibia trabecular bone is similar at 359 ± 186 MPa. Hence from a mechanical property point of view, the results obtained from polyurethane foam may not be far from those of cancellous bones in bovine and human cases.

Although the influence of crack length on the interfacial fracture toughness seems to be moderate at low phase angles, significant influence may be observed at large phase angles where shear mode becomes predominant (Fig. 8). As the measured interfacial fracture toughness seems to be dependent on crack length, it should be regarded as an apparent interfacial toughness, rather than a true material property. The fracture load represents the load required to "pull-out" the cement pedicles from the pores, hence the length of the ligament (and the crack length) will have an influence on the results. As interfacial toughness is proportional to fracture load, a crack length dependency is not unexpected. A micromechanics-based approach may be more appropriate to model the local events such as "pull-out", where alternative parameters may emerge. This is a subject of further work.

Although polyurethane foams are limited in their representation of features of human cancellous bone, they seem to be possible candidates as analogous materials with comparable mechanical properties to those of cancellous bones, and with inter-specimen variability 20–200 times lower than that for cadaveric specimens [23]. Microscopic studies also suggest that the polyurethane foams do have a sponge-like appearance with pore sizes in the order of 100–200 μm, and typical features such as "pull-out" of cement pedicles from the pores of the sawbones were also observed (Fig. 9). Preliminary work on bovine cancellous bone–cement interface seems to indicate similar types of failure mechanism, as shown in Fig. 10, although the pores in the bovine

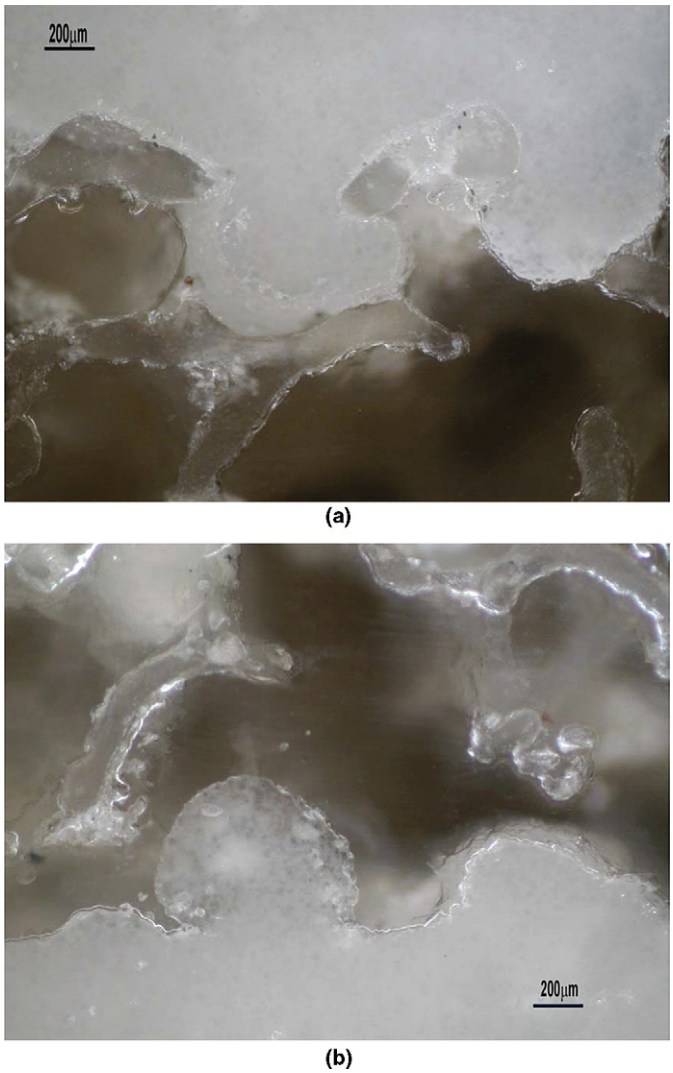

Fig. 10. Micrographs of bovine cancellous bone–cement interfaces: (a) Intact interface and (b) fractured interface at $\theta = 0°$.

bones are more irregular and larger in size, typically in the order of 1 mm. It is likely that these larger, more irregular pores would enhance interlocking between the bone and the cement, consequently higher fracture toughness may be obtained. Indeed preliminary results suggest that the interfacial fracture toughness between bovine cancellous bone and cement is about 2.5 times that of sawbone and cement at $\theta = 0°$.

Although there have been no publications on the interfacial fracture toughness between polyurethane foams and PMMA, there have been publications [5,12,14] on the bonding behaviour of PMMA to cadaveric bones. Mann et al. [5] reported that the bonding strength between human femur and cement depended on the amount of bone interdigitated with PMMA cement, with a mean fracture energy measured as 350 J/m^2 for mode I and 1000 J/m^2 for mode II, although no defects were introduced in these tests. Wang and Agrawal [12] reported interfacial fracture toughness between bovine cortical bone and PMMA to be between 38 and 52 J/m ^{2} for phase angles $-18° < \psi < 16°$; while [14] reported 44–53 J/m^2 for bovine cortical bone and two different cements at $\psi \approx 45°$. There is a significant difference in the last two sets of results, where the values of the fracture toughness obtained appear to be similar, independent of phase angle, which is known to be untrue [19]. The present results are comparable to the results from [14], with an average value of G_{IC} of 47 J/m^2 at $\psi \approx 45°$. An average value of G_{IC} of 20 J/m^2 was obtained at $|\psi| < 18°$, as opposed to

$\sim$38–52 J/m^2 from [12]. It has to be said, however, that any correlations or otherwise between these values may be coincidental, as both the modulus and the morphology of cortical bones are very different from those of the foams.

Admittedly, the morphology of the polyurethane foam is likely to have the most significant influence on the interfacial fracture toughness measured. Experiments are being carried out to examine bovine bones as well as different grades of solid and cellular foams with varied sizes of pores. Further work is also being considered where the morphology of the bone may be used in the construction of micro-mechanics model and objective Oriented Finite Element code may be used to incorporate micro-structural details in the analysis.

Acknowledgements

The work was partially funded by the Medical Research Council of UK. We are grateful for the constructive suggestions of the referees.

References

[1] Stocks GW, Freeman MHR, Evans SJW. Acetabular cup migration, prediction of aseptic loosening. J Bone Jt Surg Br 1995;77B:853–61.
[2] Thanner J. The acetabular component in total hip arthroplasty, evaluation of different fixation principles. Acta Orthop Scand 1999;70(Suppl. No. 286).
[3] Huiskes R. Failed innovation in total hip replacement. Acta Orthop Scand 1993;64:699–716.
[4] Collier JP, Michael DE, Mayor B. Mechanisms of failure of modular prostheses. Clin Orthop Rel Res 1992;285:129–39.
[5] Mann KA, Mocarski R, Damron LA, Allen MJ, Ayers DC. Mixed mode fracture response of the cement–bone interface. J Orthop Res 2001;19:1153–61.
[6] Krause WR, Krug W, Miller J. Strength of the cement–bone interface. Clin Orthop Rel Res 1982;163:290–9.
[7] MacDonad W, Swarts E, Beaver R. Penetration and shear strength of cement–bone interfaces in vivo. Clin Orthop Rel Res 1993;286:283–8.
[8] Mann KA, Werner FW, Ayers DC. Modelling the tensile behaviour of the cement–bone interface using nonlinear fracture mechanics. J Biomech Engng 1997;119:175–8.
[9] Mann KA, Werner FW, Ayers DC. Mechanical strength of the cement–bone interface is greater in shear than in tension. J Biomech 1999;32:1251–4.
[10] Kim D-G, Miller MA, Mann KA. Creep dominates tensile fatigue damage of the cement–bone interface. J Orthop Res 2004;22:633–40.
[11] Wang X, Subramaniannda R, Agrawal M. Testing of bone–biomaterial interface bonding strength: a comparison of different techniques. J Biomed mater Res 1996;33:133–8.
[12] Wang X, Agrawal M. Interfacial fracture toughness of tissue-biomaterial systems. J Biomed mater Res 1997;38:1–10.
[13] Charalambides PG, Lund J, McMeeking RM. A test specimen for determining the fracture resistance of biomaterial interfaces. J Appl Mech 1989;56:77–83.
[14] Lucksanasombool P, Higgs WA, Higgs RJED, Swain MV. Interfacial fracture toughness between bovine cortical bone and cement. Biomaterials 2003;24:1159–66.
[15] Atkinson C, Smelser RE, Sanchez J. Combined mode fracture via the cracked Brazilian disk test. Int J Fract 1982;18:279–91.
[16] Soares JB, Tang T-X. Bimaterial Brazilian specimen for determining interfacial fracture toughness. Engng Fract Mech 1998;59:57–71.
[17] Wang J-S, Suo Z. Experimental determination of interfacial toughness curves using Brazil-nut-sandwiches. Acta Metall Mater 1990;38:1279–90.
[18] Tong J, Wong KY. Mixed mode fracture in reconstructed acetabulum. In: Proceedings of 11th international conference on fracture, Turin; 2005.
[19] Rice J. Elastic fracture mechanics concepts for interfacial cracks. J Appl Mech 1988;55:98–103.
[20] Tvergaard V. Prediction of mixed mode interface crack growth using a cohesive zone model for ductile fracture. J Mech Phys Solids 2004;52:925–40.
[21] ABAQUS 6.5. Hibbitt, Karlsson&Sorensen, Inc.
[22] ASTM F-1839. Standard specification for rigid polyurethane foam for use as a standard material for testing orthopaedic devices and instruments, 2001.
[23] Cristofolini L, Viceconti M, Cappello A, Toni A. Mechanical validation of whole bone composite femur models. J Biomech 1996;29:525–35.
[24] Haddock SM, Yeh OC, Mummaneni PV, Rosenberg WS, Keaveny TM. Similarity in the fatigue behaviour of trabecular bone across site and species. J Biomech 2004;37:181–7.
[25] Keaveny TM, Hayes WC. A 20-year perspective on the mechanical properties of trabecular bone. Tran ASME J Biomech Engng 1993;115:534–42.